JACS
JOURNAL OF THE AMERICAN CHEMICAL SOCIETY
Article
pubs.acs.org/JACS

Effect of Acceptor Strength on Optical and Electronic Properties in Conjugated Polymers for Solar Applications

Oluwasegun O. Adegoke,[†] In Hwan Jung,[‡] Meghan Orr,[†] Luping Yu,[‡] and Theodore Goodson III*,[†]

[†]Departmentof Chemistry, University of Michigan, Ann Arbor, Michigan 48109, United States
[‡]Departmentof Chemistry and the James Franck Institute, The University of Chicago, Chicago, Illinois 60637, United States

Supporting Information

ABSTRACT: Four new low-bandgap electron-accepting polymers—poly(4,10-bis(2-butyloctyl)-2-(2-(2-ethylhexyl)-1,1-dioxido-3-oxo-2,3-dihydrothieno[3,4-*d*]-isothiazol-4-yl)thieno[2′,3′:5,6]pyrido[3,4-*g*]thieno[3,2-*c*]isoquinoline-5,11-(4*H*,10*H*-dione) (PNSW); poly(4,10-bis(2-butyloctyl)-2-(5-(2-ethylhexyl)-4,6-dioxo-5,6-dihydro-4*H*-thieno[3,4-*c*]pyrrol-1-yl)thieno[2′,3′:5,6]pyrido[3,4-*g*]thieno-[3,2-*c*]isoquinoline-5,11(4*H*,10*H*)-dione) (PNTPD); poly(5-(4,10-bis(2-butyl-octyl)-5,11-dioxo-4,5,10,11-tetrahydrothieno[2′,3′:5,6]pyrido[3,4-*g*]thieno[3,2-*c*]-isoquinolin-2-yl)-2,9-bis(2-decyldodecyl)anthra[2,1,9-*def*:6,5,10-*d*′*e*′*f*′]-diisoquinoline-1,3,8,10(2*H*,9*H*)-tetraone) (PNPDI); and poly(9,9-bis(2-butyloctyl)-9*H*-fluorene-bis((1,10:5,6)2-(5,6-dihydro-4*H*-cyclopenta[*b*]thiophene-4-ylidene)-malonitrile)-2-(2,3-dihydrothieno[3,4-*b*][1,4]dioxine)) (PECN)—containing thieno[2′,3′:5′,6′]pyrido[3,4-*g*]thieno[3,2-*c*]isoquinoline-5,11(4*H*,10*H*)-dione and fluorenedicyclopentathiophene dimalononitrile, were investigated to probe their structure−function relationships for solar cell applications. PTB7 was also investigated for comparison with the new low-bandgap polymers. The steady-state, ultrafast dynamics and nonlinear optical properties of all the organic polymers were probed. All the polymers showed broad absorption in the visible region, with the absorption of PNPDI and PECN extending into the near-IR region. The polymers had HOMO levels ranging from −5.73 to −5.15 eV and low bandgaps of 1.47−2.45 eV. Fluorescence upconversion studies on the polymers showed long lifetimes of 1.6 and 2.4 ns for PNSW and PNTPD, respectively, while PNPDI and PECN showed very fast decays within 353 and 110 fs. PECN exhibited a very high two-photon absorption cross section. The electronic structure calculations of the repeating units of the polymers indicated the localization of the molecular orbitals in different co-monomers. As the difference between the electron affinities of the co-monomers in the repeating units decreases, the highest occupied and lowest unoccupied molecular orbitals become more distributed. All the measurements suggest that a large difference in the electron affinities of the co-monomers of the polymers contributes to the improvement of the photophysical properties necessary for highly efficient solar cell performance. PECN exhibited excellent photophysical properties, which makes it to be a good candidate for solar cell device applications.

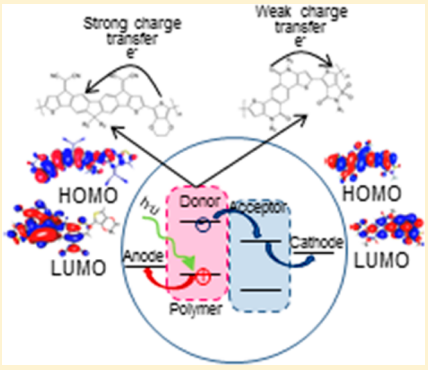

1. INTRODUCTION

The development of renewable source of energy is necessary in order to replace fossil fuels, ensure sustainability in the energy sector, and protect the environment. The search for alternative sources of energy has been ongoing for many decades.[1,2] The vast amount of energy reaching the earth from the sun has necessitated research into ways to harvest this natural energy source. Photovoltaic solar cell devices can convert sunlight into electricity. However, the most popularly used solar cells based on inorganic semiconductors are expensive and have limited deployment in the field. Recently, organic photovoltaic solar cell devices have emerged as potential alternatives to effectively utilize solar energy[3−9] because of their high abundance, flexibility, ease of production, and variety of emerging promising organic compounds for solar cell applications.[9−14] Significant improvement in the design of light-harvesting materials has led to power conversion efficiency (PCE) of organic solar cell devices reportedly reaching 10% recently.[15−17] However, to be commercially viable, it is necessary to fabricate solar cell devices with PCE over 15%.[18,19] Thus, new materials with better performance must be developed.

One strategy that has been adopted to improve PCE is the inducement of intramolecular charge transfer in organic polymers by designing conjugated donor−acceptor co-polymers.[20−27] One group of polymers, which has been developed using this approach and has been reported to have PCEs larger than 8% in photovoltaic devices, is the poly-(thienothiophene-benzodithiophene) (PTB) polymer series. These polymers contain repeating units of alternating thieno-[3,4-*b*]thiophene (TT) and benzodithiophene (BDT).[18,28−31] The highest occupied and lowest unoccupied molecular orbital (HOMO and LUMO) energy levels of the polymers were optimized by fine-tuning their structures through the addition

Received: January 8, 2015
Published: April 7, 2015

DOI: 10.1021/ja513002h
J. Am. Chem. Soc. 2015, 137, 5759−5769

of various substituents in the backbone of the polymers. Electron-donating alkyl and alkoxyl groups were substituted in the BDT unit, while electron-withdrawing esters and a fluorine atom were substituted in the TT unit in order to fine-tune the structures of the PTB polymer series. The representative polymer in the PTB series with the highest PCE is poly[[4,8-bis[(2-ethylhexyl)oxy]benzo[1,2-*b*:4,5-*b*′]dithiophene-2,6-diyl][3-fluoro-2-[(2-ethylhexyl)carbonyl]thieno[3,4-*b*]-thiophenediyl]] (PTB7).[18]

The excellent performance of PTB7 has generated intense research to understand how the structures of polymers correlate to their performance. PTB7 showed characteristics such as low-lying HOMO and LUMO energy levels, a small bandgap, good morphology of PTB7-phenyl-C_{60}-butyric acid methyl ester ($PC_{60}BM$) films, and good absorption over the entire visible and near-infrared (NIR) regions.[29,32−35] The strong electron-withdrawing effect of the TT unit from the electron-rich BDT unit, which results in a localized dipole moment in the TT unit, played an important role in the excellent photovoltaic performance of the PTB7 devices.[18] The alternating co-polymer structure concentrates the negative charge in the TT unit with the positive charge being localized in the electron-rich BDT unit. The induced charges on the TT and BDT units cause enhancement of the dipole moment in PTB7.[18] The dipole moment of PTB7 was further enhanced by the addition of fluorine as a side atom in the TT unit, which encourages a better charge transfer in the polymer chain.

Emerging organic photovoltaic materials depend on the "push−pull" concept or donor−acceptor mechanism. Carsten et al.[18] worked on different polymers with alternating BDT and TT having different electron-withdrawing substituents to investigate the push−pull mechanism. In the study, poly[(4,8-bis(octyloxy)benzo(1,2-*b*:4,5-*b*′)dithiophene-2,6-diyl)(2-((2-ethylhexyl)carbonyl)thieno(3,4-*b*)thiophenediyl)] (PTB2) did not have a fluorine atom, and PTB7 did have a fluorine atom attached to the TT unit. Poly[(4,8-bis((2-ethylhexyl)oxy)-3,7-difluorobenzo(1,2-*b*:4,5-*b*′)dithiophene-2,6-diyl)(2-((2-ethylhexyl)carbonyl)thieno(3,4-*b*)thiophenediyl)] (PTBF2) had two opposing fluorine atoms attached to the BDT unit, while poly[(4,8-bis((2-butyloctyl)oxy)benzo(1,2-*b*:4,5-*b*′)-dithiophene-2,6-diyl)(2,2′-bis(((2-butyloctyl)oxy)carbonyl)-6,6′-bithieno(3,4-*b*)thiophenediyl)] (PBB3) had two adjacent TT units in a trans conformation. These substituents were able to reduce the energy levels of the polymers because of their electron-withdrawing effect. A deep-lying HOMO energy level ensures oxidative stability of organic polymer materials.[36,37] PBB3 was found to have the best absorption in the NIR region due to the increased conjugation as a result of the additional thiophene ring. However, it showed the smallest dipolar change between the ground and excited states.[18] PTB2 and PTB7 were found to have the largest dipolar changes. The dipolar change between the ground and excited states of PBB3 was lower than those of PTB2 and PTB7 by factors of 6 and 8, respectively. The result shows that the nature and the position of electron-withdrawing substituents in the organic polymer chain affect the magnitude of the dipolar change. The position and configuration of the attached substituents play a huge role in the magnitude of the dipole moment.

The development of new organic photovoltaic polymers has focused more on the energetics of the donor polymers in bulk heterojunction (BHJ) systems because of the need to ensure a good offset between the LUMO of the donor polymer and the LUMO of the fullerene in polymer/fullerene blends. For effective charge carrier generation by exciton dissociation at the interface between the donor polymer and fullerene, the offset between the LUMO of the donor polymer and LUMO of fullerene acceptor must be at least 0.30 V.[38−40] However, it has been found recently that good charge separation in the donor polymer reduces the offset required for effective charge transfer from the donor polymer to the fullerene in a BHJ system.[18,41,42] In a study by Carsten et al.,[18] the transient absorption results of blended films of PTB7 with fullerenes showed a fast excitonic-state decay of less than 120 fs, while blends of PTBF2 and PBB3 with fullerenes showed longer excitonic decay times of 19 and 190 ps, respectively. On the other hand, the first components of the charge-separated state of PTB7, PTBF2, and PBB3 were found to be 87, 1.6, and 6 ps, respectively.[18] Based on the excitonic decay time and charge-separated state obtained in the transient absorption experiment on the polymer/fullerene blend, PTB7 showed the most efficient charge transfer and the lowest charge recombination rate. This is in spite of the fact that the energetics of the three polymers were identical, and PTB2 had even better crystallinity than PTB7. The excellent performance of PTB7 could be attributed to enhanced transition dipole moment, which increases the driving force for charge transfer from PTB7 to the fullerene acceptor and reduces the rate at which electrons and holes recombine.[18] Local dipole moment of polymers could have a great influence on the efficiency of charge transfer and ultimately the PCE of solar cell devices.

In this article, we present the results of a spectroscopic study of PTB7 and a series of low-bandgap polymers in order to elucidate why PTB7-based devices offer excellent efficiency. These low-bandgap polymers include electron-withdrawing polymers designed to serve as possible replacements of fullerene derivatives in solar cell devices.[43] Fullerenes are efficient electron acceptors because of their high electron affinity and mobility. However, they are rather expensive and also suffer from low absorption at longer wavelengths of the solar spectrum. The polymers were designed based on electron-accepting moieties, thieno[2′,3′:5′,6′]pyrido[3,4-g]thieno[3,2-*c*]isoquinoline-5,11(4H,10H)-dione (TPTI) and fluorenedicyclopentathiophene dimalononitrile (FDCPT-CN). The polymers investigated are the low-bandgap polymers poly(4,10-bis(2-butyloctyl)-2-(2-(2-ethylhexyl)-1,1-dioxido-3-oxo-2,3-dihydrothieno[3,4-*d*]isothiazol-4-yl)thieno[2′,3′:5,6]pyrido-[3,4-*g*]thieno[3,2-*c*]isoquinoline-5,11(4*H*,10*H*-dione) (PNSW), poly(4,10-bis(2-butyloctyl)-2-(5-(2-ethylhexyl)-4,6-dioxo-5,6-dihydro-4*H*-thieno[3,4-*c*]pyrrol-1-yl)thieno-[2′,3′:5,6]pyrido[3,4-*g*]thieno[3,2-*c*]isoquinoline-5,11-(4*H*,10*H*)-dione) (PNTPD), and poly(5-(4,10-bis(2-butyl-octyl)-5,11-dioxo-4,5,10,11-tetrahydrothieno[2′,3′:5,6]pyrido-[3,4-*g*]thieno[3,2-*c*]isoquinolin-2-yl)-2,9-bis(2-decyldodecyl)-anthra[2,1,9-*def*:6,5,10-*d*′*e*′*f*′]diisoquinoline-1,3,8,10(2*H*,9*H*)-tetraone) (PNPDI), which have TPTI within their structures, and poly(9,9-bis(2-butyloctyl)-9*H*-fluorene-bis((1,10:5,6)2-(5,6-dihydro-4*H*-cyclopenta[*b*]thiophene-4-ylidene)-malonitrile)-2-(2,3-dihydrothieno[3,4-*b*][1,4]dioxine)) (PECN), which contains FDCPT-CN in its structure. Detailed fluorescence dynamics and nonlinear properties of these polymers are also presented to offer insight about their photophysics. The results suggest that the efficiency of the charge-transfer processes increases as the difference in the electron affinities of the co-monomers in the polymers increases. As a result, PECN and PTB7, which have alternating electron-donating and electron-withdrawing co-monomers,

DOI: 10.1021/ja513002h
J. Am. Chem. Soc. 2015, 137, 5759−5769

were found to have the best charge-transfer abilities among the investigated polymers.

2. EXPERIMENTAL SECTION

2.1. Materials. The synthesis of PTB7 and the polymers were carried out by Stille polycondensation method, and purification was done by column chromatography.[30,43] The polymers were characterized by using ^{1}H NMR, ^{13}C NMR, and mass spectroscopy (MALDI-TOF). The molecular weights of the polymers are shown in Table 1. The samples were dissolved in spectroscopic-grade chloroform (Sigma-Aldrich, spectrophotometric grade). The optical densities of the samples were below 0.5 in order to avoid re-absorption during ultrafast measurements.

2.2. Steady-State Measurements. The steady-state measurements of the samples were performed at room temperature. Concentrations ranging from 1.7×10^{-7} to 5.1×10^{-7} M were used for the samples. The samples were placed in 4 mm quartz cuvettes. Steady-state absorbance spectra were measured using an Agilent 8432 UV−visible absorption spectrophotometer. The emission spectrum measurements were performed with a Fluoromax-2 spectrophotometer. To ensure that there was no appreciable photo-degradation during the fluorescence lifetime measurements, absorption spectra measurements were taken before and after each measurement. There was no difference between the absorption spectra taken before and after the fluorescence lifetime measurements. The quantum yields of the samples were calculated using a known procedure[44,45] with 5,10,15,20-tetraphenyl-21*H*,23*H*-porphine (TPP) dissolved in toluene ($\phi_f = 0.11$) used as standard.[46] The quantum yields were measured at excitation wavelength of 514 nm.

2.3. Fluorescence Lifetime Measurements. The time-resolved fluorescence experiments were performed using a fluorescence setup that had previously been described.[47−50] Mode-locked Ti-sapphire femtosecond laser (Spectra Physics Tsunami) was used to generate 80 fs pulses at 800 nm wavelength with a repetition rate of 82 MHz. This mode-locked laser was pumped by a 532 nm continuous light output from another laser (Spectra Physics Millennia), which has a gain medium of neodymium-doped yttrium vanadate (Nd:YVO_4). An excitation pulse of 400 nm was generated by a second harmonic β-barium borate crystal, and the residual 800 nm beam was made to pass through a computer-controlled motorized optical delay line. The polarization of the excitation beam was controlled by a berek compensator. The power of the excitation beam varied between 17 and 20 mW. The fluorescence emitted by the sample was up-converted by a nonlinear crystal of β-barium borate by using the residual 800 nm beam, which had been delayed by the optical delay line with a gate step of 6.25 fs. This procedure enabled the fluorescence to be measured temporally. The monochromator is used to select the wavelength of the up-converted beam of interest, and the selected beam is detected by a photomultiplier tube (R152P, Hamamatsu, Hamamatsu City, Japan). The photomultiplier tube converts the detected beam into photon counts, which can be read from a computer. Coumarin 153 and Cresyl violet dyes were used for calibrating the laser. The instrument response function (IRF) has been determined from the Raman signal of water to have a width of 110 fs.[51] Lifetimes of fluorescence decay were obtained by fitting the fluorescence decay profile with multi-exponential decay functions convoluted with IRF in MATLAB and Origin 8.

For PNSW and PNTPD having lifetimes in the nanosecond range, fluorescence lifetimes were measured using time-correlated single-photon counting (TCSPC) technique, which has been described previously.[52] The laser used for the TCSPC measurement was a Kapteyn Murnane (KM) mode-locked Ti-sapphire laser. The output beam from the KM laser was at 800 nm wavelength, with pulse duration of ∼30 fs. The output beam was frequency-doubled using a nonlinear barium borate crystal to obtain a 400 nm beam. A polarizer was used to vary the power of the 400 nm beam that excites the sample. Focus on the sample cell (quartz cuvette, 0.4 cm path length) was ensured using a lens of focal length 11.5 cm. Collection of fluorescence was done in a direction perpendicular to the incident beam into a monochromator, and the output from the monochromator was coupled to a photomultiplier tube, which converted the photons into counts.

2.4. Two-Photon Absorption (TPA) Measurements. The TPA cross sections of the polymer samples were measured by an open-aperture *z*-scan method. The nonlinear optical setup used in our study is shown in the Supporting Information (Figure S1). The generation of the 1200 nm incident beam used in the experiment has been described previously.[52,53] The Spectra Physics diode-pumped Millenia Pro generated 3.57 W, 532 nm continuous wave beam, which was used as a pump beam for Ti:sapphire regenerative oscillator (Tsunami, Spectra Physics). Ti-sapphire regenerative amplifier (Spitfire, Spectra Physics) generated 100 fs, 1 mJ pulses at 800 nm with an average power of 1 W with seed pulses from the Ti-sapphire regenerative oscillator (Tsunami, Spectra Physics) and a pump beam of 7.5 W, 532 nm from Nd:YLF laser (Spectra Physics, Empower). The incident beam was produced using an optical parametric amplifier (OPA-800C), with a wavelength range of 300−1200 nm. The incident beam was generated by the nonlinear crystal BBO in the OPA-800C using the second harmonic of the idler that was set at 1200 nm. The intensity of the incident beam was controlled by a circular variable neutral density filter. A beam splitter was used in splitting the incident beam into two for calibration purpose. A focusing lens, with a focal length of 25 cm, is placed before the sample to focus the incident beam. The transmitted beam through the sample is measured using an open-aperture detector, and the result is processed using known correlations (eqs 1 and 2)[54] in the literature to obtain the TPA cross sections of the samples.

$$T(z) = 1 - \frac{\beta I_o (1 - e^{-\alpha L})}{2^{3/2}\alpha(1 + z^2/z_o^2)} \quad (1)$$

$$T(z) = 1 - \frac{\beta I_o L}{2^{3/2}(1 + z^2/z_o^2)} \quad \text{if} \quad \alpha \ll 1 \quad (2)$$

In the equations above, I_o is the intensity of the incident beam at the focus, β is the two-photon absorption coefficient, L is the length of sample in the direction of the beam, and z is the position of the sample in the direction of the beam. The TPA cross section in the unit of GM (cm^4·s/photon·molecule) is evaluated by using eq 3.

$$\sigma_2 = \frac{\beta h\nu \times 10^3}{Nc} \quad (3)$$

2.5. Molecular Orbital Calculations. The electronic structure calculation was implemented in GAMESS (General Atomic and Molecular Electronic Structure System).[55,56] The configuration interaction singles (CIS) approach was employed in this work. CIS approach uses the restricted Hartree−Fock (RHF) theory, which generates all singly excited determinants of configuration interaction expansions. The CIS approach has the advantage of simultaneous calculation of a large number of excited states and the optimization of a desired selected state. In this study, the calculation was done for 11 excited states and optimized for the first excited state. The basis set used was 6-31G, and the initial molecular orbital guess was Hückel. The electronic structure calculation was carried out on the repeating monomers of the polymers. The structures of the monomers were drawn using ChemDraw. Methyl was used to represent the alkyl ends of the monomer in order to reduce the complexity and times of computation. The repeating monomers were modeled using Avogadro software.[57] The GAMESS extension plug-in of Avogadro was used to prepare the input files for GAMESS-US,[55,56] which was used for the molecular orbital calculations. The complexity of the building block of the monomer determines the convergence criterion used for the calculation, and it varied from 10^{-7} to 10^{-5}. Gabedit[58] was used to visualize the molecular orbital results.

3. RESULTS

3.1. Synthesis. The molecular structure of PTB7 and the detailed synthetic routes to the polymers PNSW, PNTPD,

DOI: 10.1021/ja513002h
J. Am. Chem. Soc. 2015, 137, 5759−5769

Scheme 1. Structure of PTB7 and Schematic Routes to PNSW, PNTPD, PNPDI, and PECN

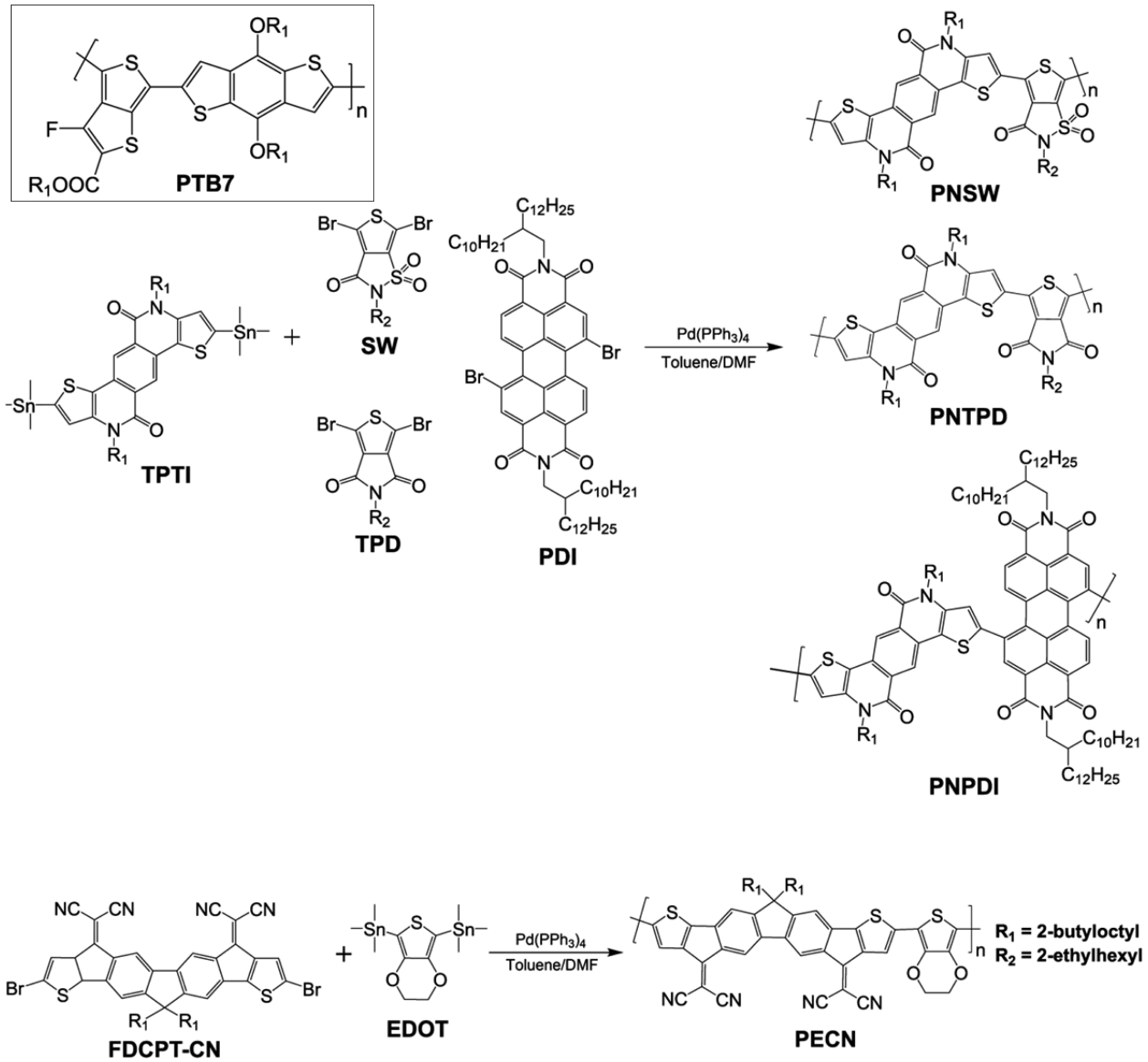

PNPDI, and PECN are provided in Scheme 1.[30,43] PNSW, PNTPD, and PNPDI were synthesized by combining electron-accepting co-monomers with stannylated TPTI. The electron-accepting co-monomers used in the synthesis of PNSW, PNTPD, and PNPDI are brominated thieno[3,4-*d*]isothiazol-3(2*H*)-one-1,1-dioxide (SW), thieno[3,4-*c*]pyrrole-4,6(5*H*)-dione (TPD), and 3,4,9,10-perylene diimide (PDI), respectively. PECN was synthesized through a similar process by combining brominated FDCPT-CN and stannylated 2,3-dihydrothieno[3,4-*b*][1,4]dioxine (EDOT).

PNSW, PNTPD, and PNPDI have the TPTI unit in their polymer chains, but they contain different electron accepting moieties in SW, TPD, and PDI, respectively. The TPD unit has an electron-withdrawing imide group, while SW has a stronger electron-withdrawing sulfonamide unit. PDI is a well-known electron accepting unit containing diimide functionality. Zhang et al. had demonstrated effective electron and charge transfer from dendritic oligothiophene (DOT) to perylene bisimide (PBI) in the literature.[59] PECN has donor−acceptor design configuration of strong electron-donating EDOT and strong electron-withdrawing FDCPT-CN moiety.

3.2. Steady-State Measurements. The steady-state absorption spectra of the investigated polymers are shown in Figure 1. A summary of the steady-state properties of the polymers is provided in Table 1. The absorbance of the polymer samples spans the entire visible spectrum. PTB7 had the highest molar absorptivity of 3.40×10^6 $M^{-1}\cdot cm^{-1}$. The excellent absorptivity of PTB7 in the NIR region, where the solar flux peaks, may be critical to the observed excellent efficiency of its photovoltaic device.[29] The absorption spectrum of PTB7 was red-shifted relative to the TPTI-based polymers. The small bandgap of PTB7 and the red-shift in the absorption spectrum of PTB7 can be attributed to the promotion of the quinoid population by the TT unit of the polymer, which leads to a concomitant decrease in bond length alternations. In addition, the presence of a strong electronegative fluorine atom and an electron-withdrawing ester in the TT co-monomer of PTB7 modulates the energy levels, consequently resulting in a small bandgap and contributing to the absorption of PTB7 at long wavelengths. Only PECN has an absorption peak at a longer wavelength than PTB7. Coincidentally, PECN consists of alternating repeating units of strong electron-withdrawing

DOI: 10.1021/ja513002h
J. Am. Chem. Soc. 2015, 137, 5759−5769

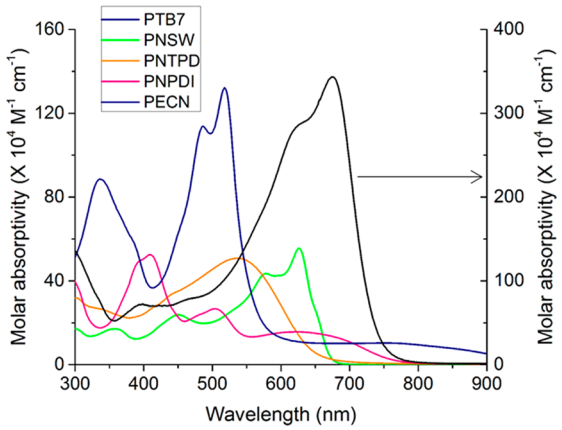

Figure 1. Absorption spectra of polymer samples. The molar absorptivity of PTB7 is denoted by the right scale.

FDCPT-CN and strong electron-donating EDOT, similar to the design motif of PTB7. PTB7 has a weak electron-donating BDT unit and a strong electron-withdrawing substituted TT. Therefore, the absorption in the IR region of PECN can be attributed to the improved conjugation in the PECN unit and strong intermolecular interaction between the electron-donating and electron-withdrawing units of PECN. The alternating donor−acceptor structure of the PTB7 and PECN enhances electron delocalization, which results in the significant red-shift relative to the other polymers. The absorption spectra of PTB7 and PECN extended to wavelengths of 800 and 900 nm, respectively.

The primary absorption peak in PTB7 was obtained at 680 nm, and this can be attributed to the $\pi-\pi^*$ interaction between the TT and BDT units. A small peak at 396 nm found in the spectrum of PTB7 can be attributed to a $S_0 \rightarrow S_1$ transition in the TT unit. PECN had the widest spectra coverage up to 900 nm, and it had its most intense peak around 518 nm. The PECN peak around 486 nm can be attributed to the $S_0 \rightarrow S_1$ transition in the EDOT unit while the intense peak at 518 nm is due to an electronic transition in the FDCPT-CN. The broad absorption peak at 753 nm can be attributed to a $\pi-\pi^*$ interaction between FDCPT-CN and EDOT. The higher energy level of the HOMO in the electron donor, EDOT, and lower energy level in the electron acceptor, FDCPT-CN, gave rise to a low bandgap (see Figure 2), and the intrachain charge transfer from the donor to the acceptor resulted in the absorption peak at 753 nm.

The onset of absorption in PNPDI was 766 nm. The proximity of the onset to the IR region is due to the presence of a strong electron-withdrawing PDI moiety in PNPDI, which extended its conjugation. There was a characteristic perylene C=C stretching mode associated with a $\pi-\pi^*$ transition.[60−63] PNPDI had an extended absorption beyond 600 nm.[64,65] The interaction between the TPTI co-monomer and PDI gave rise to an absorption peak at 626 nm. The absorption spectrum of PNPDI also appeared to mirror the PDI spectrum. There was a hypsochromic shift of the absorption peaks of PNPDI relative to the parent compound PDI with the 504 nm absorption peak experiencing up to a blue-shift of 20 nm. Relative to PNTPD, the absorption spectrum of PNSW was red-shifted because of the extra lone pair of electrons in the sulphonyl bond in SW in the structure of PNSW. There were noticeable vibronic states in the absorption spectrum of PNSW which were absent in the absorption spectrum of PNTPD.

As shown in Table 1, PTB7 had the highest molecular weight. PECN had the second highest molecular weight, and PNSW and PNTPD had identical molecular weights. The ability to form films with good morphology in solar cell device has been found to increase as the molecular weight of polymers increases.[66−68] The results of the electrochemical properties, investigated by cyclic voltammetry, are summarized in Figure 2.

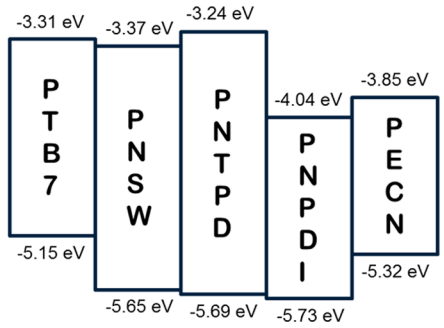

Figure 2. HOMO−LUMO energy levels of PTB7[18] and polymer samples.[43]

The TPTI-based polymers have similar HOMO energy levels, which indicate that the electron density in the HOMO may be residing in the TPTI moiety of the polymers. PNPDI, with the strongest electron-withdrawing co-monomer of PDI, has the lowest LUMO energy level out of the three polymers having TPTI. PECN has the smallest bandgap of all the investigated polymers. This is as a result of the coupled effects of the strong electron-withdrawing FDCPT-CN and strong electron-donating EDOT.

The emission spectra of the polymers are shown in Figure 3. The primary emission peaks of PNSW and PNTPD are 659 and 646 nm, respectively. These represent Stokes shifts of 33 and 109 nm for PNSW and PNTPD, respectively. The relatively bulky sulphonyl group may have reduced the energy loss due to vibration from PNSW, hence the reason for its

Table 1. Molecular Weight and Steady-State Properties of Polymers[a]

polymer	M_w (kDa)	PDI	$N_{monomer}$	λ_{abs} (nm)	λ_{em} (nm)	λ_{onset} (nm)	ϕ
PTB7	146.0	2.4	92	628, 671	736	789	0.00857
PNSW	18.5	1.61	12	359, 450, 578, 626	591, 657	679	0.286
PNTPD	18.0	1.65	12	537	576, 646	673	0.455
PNPDI	39.2	2.17	11	409, 504, 626	589,656,778	766	0.0310
PECN	52.9	2.43	23	336, 486, 518, 753	660	946	0.00154

[a] M_w is the molecular weight of the polymers, PDI is the polydispersity index, $N_{monomer}$ is the number of monomers in one molecule of the polymer, λ_{abs} is the absorption peak wavelength, λ_{em} is the emission peak wavelength, λ_{onset} is the onset of absorption, and ϕ is the quantum yield of the polymer samples, with TPP as standard and at excitation wavelength of 514 nm.

DOI: 10.1021/ja513002h
J. Am. Chem. Soc. 2015, 137, 5759−5769

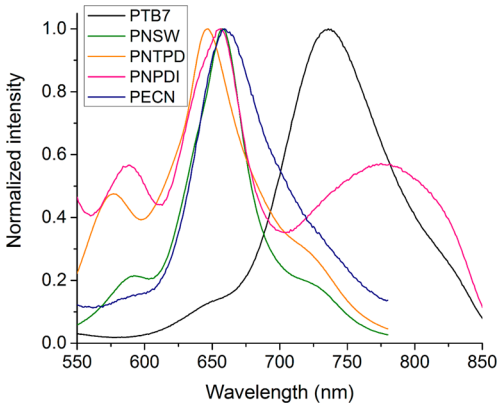

Figure 3. Emission spectra of polymer samples.

smaller Stokes shift relative to PNTPD, which contains the less bulky imide functionality. The emission peaks at 659 and 646 nm in PNSW and PNTPD, respectively, may be attributed to the electronic coupling between the donor and acceptor units in the polymers. There were secondary fluorescence peaks in the emission spectra of PNSW and PNTPD at 591 and 576 nm which can be attributed to the emission from the TPTI units. The fluorescence from PTB7 occurred at 736 nm. Relative to PNSW and PNTPD, the emission from PTB7 is red-shifted, and this red-shift can be related to the strong interaction between the BDT and TT units. PNPDI has clearly defined emission peaks at 589, 656, and 778 nm. Compared to the parent compound of PDI, the fluorescence spectrum is red-shifted and the fluorescence between 700 and 850 nm is broader.

The quantum yields were measured by exciting the samples at 514 nm using 5,10,15,20-tetraphenyl-21H,23H-porphin (TPP) dissolved in toluene (ϕ = 0.11) as a standard. The quantum yield of PTB7 was found to be 8.6×10^{-3}, and this relatively low value of quantum yield ensures that PTB7 does not lose most of its absorbed energy through a radiative pathway. Therefore, most absorbed photons by PTB7 will be converted into useful energy for solar cell applications. The TPTI-based polymers, PNSW and PNTPD, have relatively high quantum yields of 0.286 and 0.455. However, PNPDI, another polymer with TPTI co-monomer, had a low quantum yield of 3.1×10^{-2}. The fluorescence quantum yields of PDI derivatives have been reported to be close to unity.[69,70] The fluorescence quantum yield of PNPDI is much lower than the reported quantum yields of PDI derivatives. This might be as a result of the twist of the PDI core when attached to the TPTI co-monomer. This conclusion is in agreement with the result reported by Jung et al.[43] that PNPDI exhibited a distortion in its backbone structure by 48°. A similar observation was also reported by Zhang et al.[59] in a compound containing DOT and PBI, in which the distortion of the PBI core caused self-quenching of emission, thereby resulting in the reduction of the quantum yield. PECN had the lowest quantum yield of 1.54×10^{-3}, which could be due to strong charge-transfer characteristics in the polymer structure. It should be also clearly noted that charge-transfer character in conjugated polymers, such as those investigated in this contribution, has been known to limit the fluorescence quantum yield substantially. We suggest internal charge-transfer character to play a role in the quantum yield and fluorescence lifetime measurements (see below) of the investigated polymers.

3.3. Time-Resolved Fluorescence Measurements. The polymer samples were excited at 400 nm, and the fluorescence dynamics were investigated at emission wavelengths of 650 and 700 nm. The dynamics of excited-state decay was fitted to a multi-exponential decay function. The lifetimes of PNSW and PNTPD were measured using TCSPC because the lifetimes of excited-state decay for these polymers were on the order of many nanoseconds. As shown in Figure 4 and Table 2, PNPDI

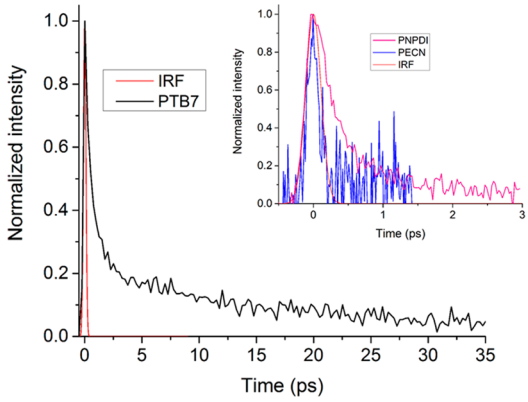

Figure 4. Decay dynamics of excited states of PTB7 at fluorescence wavelength of 700 nm Inset: Decay dynamics of excited states of polymers of PNPDI and PECN at fluorescence wavelength of 650 nm.

showed a short-lived lifetime of approximately 350 fs. PNPDI was excited in the $S_0 \rightarrow S_2$ electronic transition of perylene where the dipole moment is perpendicular to the long perylene axis. As reported in the literature, the lifetime of the parent PDI compound is 4 ns.[60,71,72] The measured lifetime of 350 fs observed in PNPDI is shorter than typical fluorescence lifetime of PDI. The short fluorescence time may be connected to the quenching effect of TPTI, which is geometrically arranged in an orthogonal orientation to PDI after excitation. As mentioned above, the existence of charge-transfer character in the polymer chain may also have a substantial influence on the fluorescence lifetime. The singlet relaxation time at fluorescence wavelength of 700 nm was also measured, and the relaxation time was found to be 6.57 ps. There was no rise time in the decay dynamics at 700 nm indicating that no energy transfer occurred at 700 nm. It is noteworthy that attempts to measure long-lived state of PNPDI did not yield appreciable fluorescence counts for analysis, which indicate that there is virtually no long-lived excited states in PNPDI. The lifetime of PECN was within the IRF, which has a full width at half-maximum (fwhm) of 110 fs. The excitation was quickly delocalized throughout the PECN structure. The fast delocalization of excitation energy in PECN resulted in the fast dynamics obtained in the fluorescence lifetime measurement. The dynamics of PTB7 singlet-state decay at fluorescence wavelength of 700 nm was fitted to a biexponential decay function. The short decay component has a lifetime of 540 fs, and there was a long-lived component of 11 ps (see Figure 4). The short component of the decay contributed about 78% of the depopulation of the excited states. The short component of 540 fs can be ascribed to internal conversion.

Shown in Figure 5 are the decay dynamics of PNSW and PNTPD, as measured by the TCSPC experiment. The decays were fitted to biexponential decay function. The lifetime of PNSW was found to have fully relaxed after 1.57 ns while the lifetime of PNTPD does not relax until after 2.40 ns. Both

DOI: 10.1021/ja513002h
J. Am. Chem. Soc. 2015, 137, 5759−5769

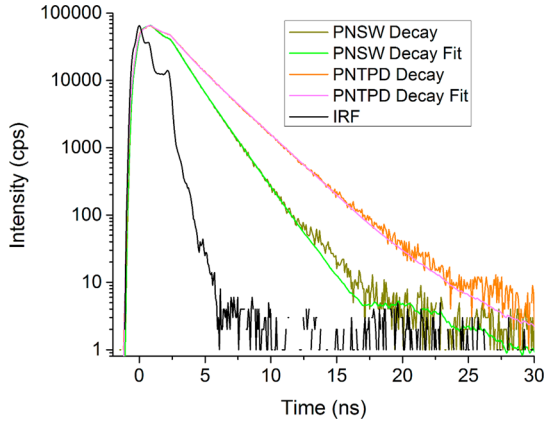

Figure 5. Decay dynamics of excited states of PNSW and PNTPD at fluorescence wavelength of 650 nm.

PNSW and PNTPD consist of electron-withdrawing co-monomers, and the long-lived state may have been as a result of absence of a pathway for fast delocalization and relaxation of the excitation energy. PTB7 and PECN each had a donor−acceptor building block, which ensures a fast energy delocalization, and TPTI may have acted as a quenching unit for the fluorescence of PDI in PNPDI. These results appear to be consistent with the quantum yields obtained for the samples in which more fluorescent polymers have longer relaxation times. A summary of the fluorescence lifetimes of the polymers is given in Table 2.

Table 2. Fluorescence Lifetimes of Polymer Samples

polymer	τ_1 (ps)	τ_2 (ps)
PTB7	0.54	11.0
PNSW	690	1570
PNTPD	900	2400
PNPDI	0.353	
PECN	<0.110	

The fluorescence lifetime measurements of the polymers indicate that the fluorescence lifetime is inversely proportional to the difference in the electron affinities of the co-monomers in the polymers. PECN, which had the fastest fluorescence dynamics, has a very good electron-donating EDOT and very strong electron-withdrawing FDCPT-CN. Therefore, there is a great difference in the electron affinities of the co-monomers in PECN. PTB7 also has a similar backbone as PECN except that the electron-donating unit, BDT in PTB7 is not as strong as EDOT. PNSW and PNTPD both have electron-withdrawing units of varying degrees coupled together. The difference in the electron affinities of the co-monomers in PNSW is however higher than in PNTPD because of the presence of the sulphonyl unit. PNPDI is the only exception to the observation, and this may be as a result of the parallel spatial arrangement of the TPTI and PDI co-monomers in PNPDI, which causes self-quenching of fluorescence.

3.4. Two-Photon Absorption. The TPA cross sections of the investigated polymers were measured using the open-aperture z-scan method. This technique involves the measurement of the transmission through the samples as a function of the z-position with respect to the focal point at $z = 0$ (see Figure S1 in Supporting Information). The TPA cross section measurement is based on the correlation between the transmittance and TPA cross section described in the previous section of this article.[54] Styryl 9M was used as a standard in the determination of TPA cross sections of the polymers. The TPA cross sections of PNSW, PNTPD, PNPDI, PECN, and PTB7 were measured as 3.30×10^4, 2.92×10^4, 4.84×10^4 , 19.04×10^4, and 9.60×10^4 GM, respectively. All the investigated polymers were studied at incident wavelength of 1200 nm except PTB7, which was studied at 1250 nm. PECN and PTB7 have the highest two photon absorption cross sections because of the presence of repeating donor−acceptor units in their structures which introduce nonlinearity and increase potential for charge transfer. PECN has a strong electron-donating EDOT co-monomer and a strong electron-withdrawing FDCPT-CN co-monomer, while PTB7 has a weak electron-donating BDT co-monomer and a strong electron-withdrawing TT co-monomer. This donor−acceptor backbone ensures that electron transfer from the donor group to the acceptor group takes place efficiently. The TPA cross section increases as the transition dipole moment increases and charge transfer becomes more efficient. Therefore, the high TPA cross section of PTB7 and PECN can be directly linked to the design motif of the two polymers. Unlike PTB7 and PECN, the other polymers have combinations of monomers with identical strengths of electron-withdrawing ability and therefore could not take advantage of the push−pull mechanism that enhances the TPA cross section. The TPA cross section of PECN may have been additionally enhanced by the presence of the dicyanoyinyl group in its polymer chain. Dicyanoyinyl groups have been found to enhance TPA cross section due to the presence of delocalized electrons in the dicyanoyinyl bond.[73−75]

We are interested in finding the contribution of each conjugation unit in each of the polymer chain to the TPA cross section. Bhatta et al.[33] found the number of monomers in the conjugating unit of PTB7 using the density functional theory calculation to be around 12 with a conjugation length of 147 Å. However, Niklas et al.[76] reported a shorter conjugation length of 40 Å and a conjugating unit of 3−4 monomers. In this article, we use a conservative estimate of 6 monomers for the conjugating unit of PTB7 and 3 units for the other polymers. By scaling the TPA cross section of PTB7 by the number of monomers in the conjugating unit, the contribution of the monomer to the TPA cross section is found to be 1.60×10^4 GM. The contributions of the monomer of PNSW, PNTPD, PNPDI, and PECN to the TPA cross section were calculated to be 1.10×10^4, 0.97×10^4, 1.61×10^4, and 6.34×10^4 GM, respectively. The results of the TPA properties of the polymers are summarized in Table 3.

The TPA cross section is highly dependent on the transition dipole moment. The TPA cross section is enhanced for conjugated systems possessing large transition dipole moments as well as large difference between the dipole moments in the ground and excited states. The transition dipole moments of the monomers in the building blocks of the polymers, given in

Table 3. TPA Properties of PTB7 and the Polymers

sample	δ ($\times 10^4$ GM)	δ/monomer ($\times 10^4$ GM)	calcd transition dipole of monomer (D)
PTB7	9.60	1.60	6.77
PNSW	3.30	1.10	9.77
PNTPD	2.92	0.97	2.08
PNPDI	4.84	1.61	1.72
PECN	19.04	6.34	4.86

DOI: 10.1021/ja513002h
J. Am. Chem. Soc. 2015, 137, 5759−5769

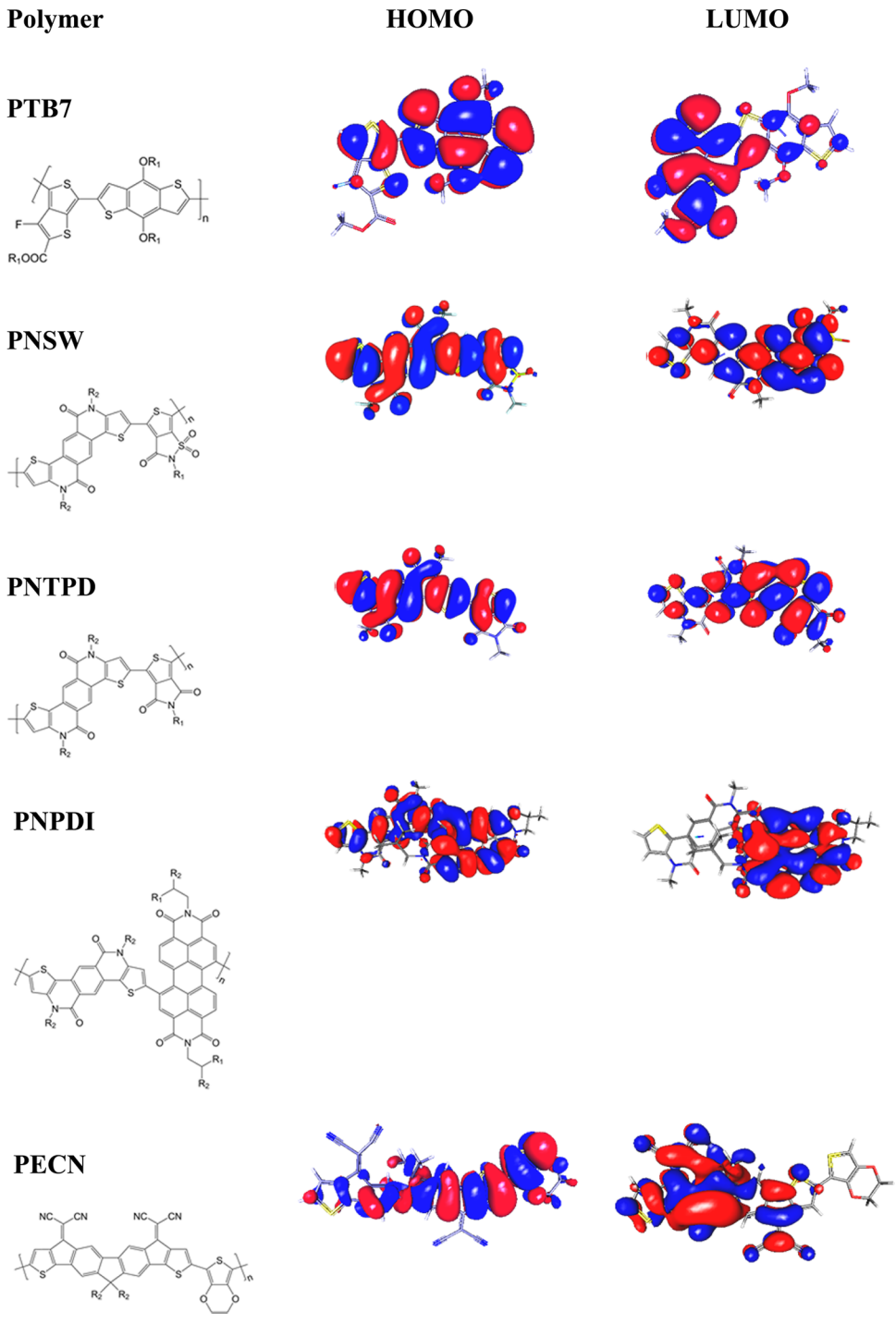

Figure 6. Molecular orbitals of the repeating monomers in the polymers.

Table 3, were obtained from the electronic structure calculations implemented in GAMESS software. The calculated transition dipole moment of PNSW was greater than those of the monomers of the other investigated polymers. The high transition dipole moment may be due to the good electron-withdrawing effect of the sulphonyl group in PNSW. However, a similar trend was not observed in the experimentally determined TPA cross section of the PNSW polymer relative to the other investigated polymers. The steric hindrance of the sulfonyl group between monomers of PNSW may have limited the experimentally measured TPA cross section. PECN and PTB7, with alternating donor−acceptor building blocks, have the higher calculated transition dipole moment and TPA cross section relative to the other investigated polymers.

3.5. Electronic Structure Calculations. The molecular orbital calculation results suggest that the HOMO energy level is concentrated at the electron-donating ends while the LUMO energy level is concentrated at the electron-withdrawing ends of the monomers of PTB7 and PECN. The localization of the molecular orbitals in different regions of the donor−acceptor co-polymers ensures that the HOMO and LUMO energy levels of the co-polymers can be turned independently. This provides the chance for further modification and improvement of the co-polymers. Only monomers of PTB7 and PECN showed

DOI: 10.1021/ja513002h
J. Am. Chem. Soc. 2015, 137, 5759−5769

appreciable localization of HOMO and LUMO in different moieties. In PTB7, the HOMO was localized on the BDT moiety while the LUMO was concentrated on the TT moiety. The presence of fluorine and esters on TT ensures that the LUMO was effectively pulled toward the TT end of the monomer of PTB7. A similar scenario was observed in PECN, in which the HOMO was localized in the EDOT moiety while the LUMO was localized in FDCPT-CN. However, the HOMO can also be seen to have extended to some part of FDCPT-CN. Therefore, the localization of the energy levels in PECN was not as pronounced as it was in PTB7. The localization of the energy levels in different moieties of the monomers provides the needed driving force for the delocalization of excited electrons and the formation of quinoid mesomeric structures through the push−pull mechanism in the donor−acceptor system. The quinoid structure influences the carbon−carbon single bond between the electron-donating and electron-withdrawing moieties to adopt more double bond character, and the bond length alternation decreases. The quinoid structure improves the conjugation in the organic systems and enhances electron transfer. Effective conjugation and electron transfer in organic systems lead to a red-shift of the absorption spectrum. This conclusion supports the results of the absorption spectra (see Figure 1), in which light harvesting in PTB7 and PECN extended to wavelengths of 800 and 900 nm, respectively, further to the NIR region than any of the other absorption spectrum of any of other investigated polymers. Good intermolecular coupling between the two dipolar ends of PTB7 and PECN enhances the absorption of light in the NIR region. In addition, good orbital mixing and redistribution of the HOMO and LUMO energy levels of PTB7 and PECN also resulted in narrow bandgaps shown in Figure 2.

In PNSW and PNTPD, the HOMO and LUMO energy levels were distributed throughout their entire monomers. In contrast to PTB7 and PECN, the monomers of PNSW and PNTPD consist of two electron-withdrawing units. Therefore, the difference in the electron affinities between the two units in each of PNSW and PNTPD is not as significant as the difference in the electron affinities in the moieties contained in PTB7 and PECN. The TPTI unit is a slightly stronger electron-withdrawing unit than the SW and TPD units in PNSW and PNTPD, respectively, resulting in a small bias of the HOMO energy level for the TPTI unit. PNSW and PNTPD cannot effectively utilize the push−pull mechanism to transfer charge because of identical electron affinities of their constituent moieties, which caused the HOMO and LUMO energy levels to be better distributed throughout monomers than PTB7 and PECN. These electronic results agree with the findings in the absorption spectra and bandgaps of PNSW and PNTPD as shown in Figures 1 and 2, respectively. The absorption spectra of PNSW and PNTPD only extended to approximately 700 nm, with the absorption peaks at 626 and 537 nm, respectively. PNSW and PNTPD also had the largest bandgaps because the HOMO and LUMO energy levels could not redistribute effectively to reduce the bandgap. The reduction in the driving force for charge transfer in PNSW and PNTPD could have played a big role in the long fluorescence lifetimes of the two polymers. On the other hand, there is a good driving force for charge transfer in PTB7 and PECN because of the localization of HOMO and LUMO energy levels, and this was evident in the very short fluorescence lifetimes of the two polymers. PNPDI is composed of two electron-withdrawing moieties in PDI and TPTI, but the electron-withdrawing strength of PDI is greater than that of TPTI. Thus, the LUMO was concentrated on the PDI moiety while the HOMO was more spread out in the PNPDI monomer. PNPDI had a spatial geometrical orientation which has TPTI lying in a parallel plane to PDI. The parallel nature of the HOMO and LUMO of TPTI and PDI in PNPDI must have contributed to the observed fluorescence quenching in the fluorescence lifetime measurements of PNPDI. Shown in Figure 6 are the HOMO and LUMO distribution of the repeating monomers in each of the polymers.

The trend observed in the TPA cross sections of the polymers can be explained by the electronic structure calculation results. It appears that for greater distribution of the electron density throughout the backbone of the monomers, the lower the TPA cross section. As a result, PTB7 and PECN have the highest TPA cross sections because of the localized nature of their energy levels at different ends of their monomers. The localization of the energy levels in PNPDI is not as evident as in PECN and PTB7 but also not as distributed as in the cases of PNSW and PNTPD. Therefore, PNPDI has an intermediate TPA cross section between those of PECN and PTB7 on one end and PNSW and PNTPD on the other end. Therefore, the TPA cross section, along with the electronic structure calculation results, can be used as a predictive tool for the charge-transfer characteristics of photovoltaic polymer materials.

As shown in Table 4, PTB7 was estimated to have excitation energy of 4.16 eV. This energy was more than the excitation energies for all other monomers. However, the cyclic voltammetry results indicated that the bandgap of PTB7 was smaller than the bandgaps of PNSW and PNTPD. The bandgap of a polymer decreases as the number of monomers in the conjugation length of the polymer increases. Therefore, the combined results of the cyclic voltammetry and the electronic structure calculations indicate that PTB7 has a conjugation length that extends beyond one monomer, which was considered in the electronic structure calculation. This conclusion is consistent with the performance of PTB7 in solar cell device. Extended conjugation is essential for effective charge transfer and ultimately good solar cell performance. The trend in the excitation energies of the other monomers was consistent with the cyclic voltammetry results shown in Figure 2.

Table 4. Electronic Properties of the Repeating Monomers of the Polymers Obtained from Electronic Calculation Using GAMESS

monomer	excitation energy (eV)	ground-state dipole (D)	transition dipole (D)
PTB7	4.16	4.17	6.77
PNSW	3.66	4.23	9.77
PNTPD	3.80	3.28	2.08
PECN	2.32	3.52	1.72
PNPDI	2.33	3.83	4.86

PECN, just like PTB7, has an alternating donor−acceptor backbone. PECN showed a wide and intense absorption band, low quantum yield, and high TPA cross section. PECN also showed a localization of the HOMO and LUMO energy levels in different moieties of its monomer. These are properties that are essential for good solar cell performance. PNSW and PNTPD, on the other hand, have moieties with identical

DOI: 10.1021/ja513002h
J. Am. Chem. Soc. 2015, 137, 5759−5769

electron affinities. The closeness in the electron-withdrawing abilities of the co-monomers of PNSW and PNTPD causes generated charges during excitation to be trapped in the polymer chain and charge-transfer process to be hindered. Therefore, there is a direct correlation between the structural backbone of the polymer and their photophysical properties, and thus photovoltaic performance, in organic photovoltaic systems. It will be worthwhile to investigate PECN as a donor material in a solar cell device. It is expected that PECN will offer a good PCE in organic photovoltaic device and will further confirm the conclusion of this article that having a backbone of alternating donor−acceptor co-polymer is the best approach to design new solar cell materials.

4. CONCLUSIONS

PTB7, which is one of the most efficient organic solar cell materials, and other novel conjugated organic polymers were investigated using linear, nonlinear, and ultrafast spectroscopic techniques. The new conjugated organic polymers have different design motifs and electron-withdrawing substituents. The photophysical results of the new polymers were compared to those of PTB7. The polymers with the donor−acceptor design motif had the greatest TPA cross section, greatest dipolar change, most intense absorption in the visible spectrum and the widest spectral absorption band. PTB7 and PECN had absorption spectra extending from 300 to 800 and 900 nm, respectively. PECN has the smallest bandgap of all the investigated polymers. This is as a result of the coupled effects of the strong electron-withdrawing FDCPT-CN and strong electron-donating EDOT. The fluorescence lifetime measurements of the polymers indicate that the fluorescence lifetime is inversely proportional to the difference in the electron affinities of the co-monomers in the polymers. PECN, which had the fastest fluorescence dynamics, has a very good electron-donating EDOT and very strong electron-withdrawing FDCPT-CN. The nonlinear spectroscopic measurements indicated that PECN and PTB7 have high TPA cross sections. PECN and PTB7, which have alternating electron-donating and electron-withdrawing co-monomers, were found to have the best charge-transfer abilities among the investigated polymers. Therefore, there will be effective charge transfer in PECN and PTB7 because of the direct correlation between TPA cross section and effectiveness of charge transfer. The electronic structure calculations in the polymers indicate that the HOMO and LUMO are localized in different moieties contained in PTB7 and PECN, which enables the polymers to take advantage of the push−pull" mechanism to transfer photo-generated charges effectively. In the other investigated polymers, the HOMO and LUMO were distributed throughout the monomer. From these results it was found that PECN had photophysical properties very similar to PTB7, and thus PECN will be a good candidate for solar cell applications.

■ ASSOCIATED CONTENT

Supporting Information

Cyclic voltammograms, UV−visible absorption spectra, thermogravimetric analysis, and gel permeation chromatography of polymers as well as the schematic of the nonlinear setup. This material is available free of charge via the Internet at http://pubs.acs.org.

■ AUTHOR INFORMATION

Corresponding Author

*tgoodson@umich.edu

Notes

The authors declare no competing financial interest.

■ ACKNOWLEDGMENTS

For T.G.III, this material is based upon work supported by the U.S. Department of Energy, Office of Science, Office of Basic Energy Sciences, Photochemistry, via Grant DE-SC0012482. L.Y. acknowledges support by the U.S. Department of Energy, No. DE-SC0000957.

■ REFERENCES

(1) Loferski, J. J. *Prog. Photovoltaics* **1993**, *1*, 67.
(2) Lodhi, M. A. K. *Energy Convers. Manag.* **1997**, *38*, 1881.
(3) Spanggaard, H.; Krebs, F. C. *Sol. Energy Mater. Sol. Cells* **2004**, *83*, 125.
(4) Benanti, T. L.; Venkataraman, D. *Photosynth. Res.* **2006**, *87*, 73.
(5) Hoppe, H.; Sariciftci, N. S. *J. Mater. Res.* **2004**, *19*, 1924.
(6) Goetzberger, A.; Hebling, C.; Schock, H.-W. *Mater. Sci. Eng., R* **2003**, *40*, 1.
(7) Brabec, C. J.; Sariciftci, N. S.; Hummelen, J. C. *Adv. Funct. Mater.* **2001**, *11*, 15.
(8) Sariciftci, N. S. *Mater. Today* **2004**, 36.
(9) Darling, S. B.; You, F. *RSC Adv.* **2013**, *3*, 17633.
(10) Nunzi, J. *C. R. Phys.* **2002**, *3*, 523.
(11) Scharber, M. C.; Sariciftci, N. S. *Prog. Polym. Sci.* **2013**, *38*, 1929.
(12) Shaheen, S. E.; Radspinner, R.; Peyghambarian, N.; Jabbour, G. E. *Appl. Phys. Lett.* **2001**, *79*, 2996.
(13) Zhan, X.; Zhu, D. *Polym. Chem.* **2010**, *1*, 409.
(14) Xue, J. *Polym. Rev.* **2010**, *50*, 411.
(15) You, J.; Dou, L.; Yoshimura, K.; Kato, T.; Ohya, K.; Moriarty, T.; Emery, K.; Chen, C.-C.; Gao, J.; Li, G.; Yang, Y. *Nat. Commun.* **2013**, *4*, 1.
(16) Liu, Y.; Chen, C.-C.; Hong, Z.; Gao, J.; Michael Yang, Y.; Zhou, H.; Dou, L.; Li, G.; Yang, Y. *Sci. Rep.* **2013**, *3*, 3356.
(17) Zhang, G.; Bala, H.; Cheng, Y.; Shi, D.; Lv, X.; Yu, Q.; Wang, P. *Chem. Commun.* **2009**, 2198.
(18) Carsten, B.; Szarko, J. M.; Son, H. J.; Wang, W.; Lu, L.; He, F.; Rolczynski, B. S.; Lou, S. J.; Chen, L. X.; Yu, L. *J. Am. Chem. Soc.* **2011**, *133*, 20468.
(19) Kalowekamo, J.; Baker, E. *Sol. Energy* **2009**, *83*, 1224.
(20) Havinga, E. E.; ten Hoeve, W.; Wynberg, H. *Polym. Bull.* **1992**, *29*, 119.
(21) Heeger, A. J. *Chem. Soc. Rev.* **2010**, *39*, 2354.
(22) Yuen, J. D.; Wudl, F. *Energy Environ. Sci.* **2013**, *6*, 392.
(23) Lei, T.; Wang, J.-Y.; Pei, J. *Acc. Chem. Res.* **2014**, *47*, 1117.
(24) Zhuang, W.; Bolognesi, M.; Seri, M.; Henriksson, P.; Gedefaw, D.; Kroon, R.; Jarvid, M.; Lundin, A.; Wang, E.; Muccini, M.; Andersson, M. R. *Macromolecules* **2013**, *46*, 8488.
(25) Owczarczyk, Z. R.; Braunecker, W. A.; Garcia, A.; Larsen, R.; Nardes, A. M.; Kopidakis, N.; Ginley, D. S.; Olson, D. C. *Macromolecules* **2013**, *46*, 1350.
(26) Bronstein, H.; Frost, J. M.; Hadipour, A.; Kim, Y.; Nielsen, C. B.; Ashraf, R. S.; Rand, B. P.; Watkins, S.; Mcculloch, I. *Chem. Mater.* **2013**, *25*, 277.
(27) Kularatne, R. S.; Magurudeniya, H. D.; Sista, P.; Biewer, M. C.; Stefan, M. C. *J. Polym. Sci. Part A, Polym. Chem.* **2013**, *51*, 743.
(28) Liang, Y.; Luping, Y. *Acc. Chem. Res.* **2010**, *43*, 1227.
(29) Liang, Y.; Xu, Z.; Xia, J.; Tsai, S.-T.; Wu, Y.; Li, G.; Ray, C.; Yu, L. *Adv. Mater.* **2010**, *22*, E135.
(30) Liang, Y.; Feng, D.; Wu, Y.; Tsai, S.-T.; Li, G.; Ray, C.; Yu, L. *J. Am. Chem. Soc.* **2009**, *131*, 7792.
(31) Liang, Y.; Wu, Y.; Feng, D.; Tsai, S.-T.; Son, H.-J.; Li, G.; Yu, L. *J. Am. Chem. Soc.* **2009**, *131*, 56.

DOI: 10.1021/ja513002h
J. Am. Chem. Soc. 2015, 137, 5759−5769

(32) Jin, Z.; Gehrig, D.; Dyer-smith, C.; Heilweil, E. J.; Laquai, F.; Bonn, M.; Turchinovich, D. *J. Phys. Chem. Lett.* **2014**, *5*, 3662.
(33) Bhatta, R. S.; Perry, D. S.; Tsige, M. *J. Phys. Chem. A* **2013**, *117*, 12628.
(34) Ito, M.; Palanisamy, K.; Kumar, A.; Murugesan, V. S.; Shin, P.-K.; Tsuda, N.; Yamada, J.; Ochiai, S. *Int. J. Photoenergy* **2014**, *2014*, 1.
(35) He, X.; Mukherjee, S.; Watkins, S.; Chen, M.; Qin, T.; Thomsen, L.; Ade, H.; Mcneill, C. R. *J. Phys. Chem. C* **2014**, *118*, 9918.
(36) Beatrup, D.; Wade, J.; Biniek, L.; Bronstein, H.; Hurhangee, M.; Kim, J.-S.; McCulloch, I.; Durrant, J. R. *Chem. Commun.* **2014**, *50*, 14425.
(37) Lim, B.; Baeg, K.-J.; Jeong, H.-G.; Jo, J.; Kim, H.; Park, J.-W.; Noh, Y.-Y.; Vak, D.; Park, J.-H.; Park, J.-W.; Kim, D.-Y. *Adv. Mater.* **2009**, *21*, 2808.
(38) Hedström, S.; Henriksson, P.; Wang, E.; Andersson, M. R.; Persson, P. *Phys. Chem. Chem. Phys.* **2014**, *16*, 24853.
(39) Mola, G. T.; Abera, N. *Phys. B* **2014**, *445*, 56.
(40) Servaites, J. D.; Ratner, M. A.; Marks, T. J. *Appl. Phys. Lett.* **2009**, *95*, 163302.
(41) Gondek, E.; Kityk, I. V.; Danel, A. *Mater. Chem. Phys.* **2008**, *112*, 301.
(42) Chi, C.-Y.; Chen, M.-C.; Liaw, D.-J.; Wu, H.-Y.; Huang, Y.-C.; Tai, Y. *ACS Appl. Mater. Interfaces* **2014**, *6*, 12119.
(43) Jung, I. H.; Lo, W.-Y.; Jang, J.; Chen, W.; Zhao, D.; Landry, E. S.; Lu, L.; Talapin, D. V.; Yu, L. *Chem. Mater.* **2014**, *26*, 3450.
(44) Maciejewski, A.; Steer, R. P. *J. Photochem.* **1986**, *35*, 59.
(45) Furgal, J. C.; Jung, J. H.; Goodson, T., III; Laine, R. M. *J. Am. Chem. Soc.* **2013**, *135*, 12259.
(46) Seybold, P. G.; Gouterman, M. *J. Mol. Spectrosc.* **1969**, *31*, 1.
(47) Adegoke, O. O.; Ince, M.; Mishra, A.; Green, A.; Varnavski, O.; Mart, M. V.; Ba, P.; Goodson, T. *J. Phys. Chem. C* **2013**, *117*, 20912.
(48) Varnavski, O.; Samuel, I. D. W.; Pålsson, L.-O.; Beavington, R.; Burn, P. L.; Goodson, T. *J. Chem. Phys.* **2002**, *116*, 8893.
(49) Varnavski, O.; Yan, X.; Mongin, O.; Blanchard-Desce, M.; Goodson, T. *J. Phys. Chem. C* **2007**, *111*, 149.
(50) Varnavski, O.; Leanov, A.; Liu, L.; Takacs, J.; Goodson, T., III *J. Phys. Chem. B* **2000**, *104*, 179.
(51) Flynn, D. C.; Ramakrishna, G.; Yang, H.; Northrop, B. H.; Stang, P. J.; Goodson, T. G., III *J. Am. Chem. Soc.* **2010**, *132*, 1348.
(52) Bhaskar, A.; Ramakrishna, G.; Lu, Z.; Twieg, R.; Hales, J. M.; Hagan, D. J.; Van Stryland, E.; Goodson, T. *J. Am. Chem. Soc.* **2006**, *128*, 11840.
(53) Yau, S. H.; Abeyasinghe, N.; Orr, M.; Upton, L.; Varnavski, O.; Werner, J. H.; Yeh, H.-C.; Sharma, J.; Shreve, A. P.; Martinez, J. S.; Goodson, T. *Nanoscale* **2012**, *4*, 4247.
(54) Nag, A.; De, A. K.; Goswami, D. *J. Phys. B At. Mol. Opt. Phys.* **2009**, *42*, 065103.
(55) Schmidt, M. W.; Baldridge, K. K.; Boatz, J. A.; Elbert, S. T.; Gordon, M. S.; Jensen, J. H.; Koseki, S.; Matsunaga, N.; Nguyen, K. A.; Su, S.; Windus, T. L.; Dupuis, M.; Montgomery, J. A. *J. Comput. Chem.* **1993**, *14*, 1347.
(56) Gordon, M. S.; Schmidt, M. W. In *Theory and Applications of Computational Chemistry: The First Forty Years*; Dykstra, C. E., Frenking, G., Kim, K. S., Scuseria, G. E., Eds.; Elsevier: Amsterdam, 2005; pp 1167−1189.
(57) Hanwell, M. D.; Curtis, D. E.; Lonie, D. C.; Vandermeersch, T.; Zurek, E.; Hutchison, G. R. *J. Cheminform.* **2012**, *4*, 1.
(58) Allouche, A. *J. Comput. Chem.* **2011**, *32*, 174.
(59) Zhang, J.; Fischer, M. K. R.; Bäuerle, P.; Goodson, T., III *J. Phys. Chem. B* **2013**, *117*, 4204.
(60) Huang, C.; Barlow, S.; Marder, S. R. *J. Org. Chem.* **2011**, *76*, 2386.
(61) Kozma, E.; Kotowski, D.; Catellani, M.; Luzzati, S.; Famulari, A.; Bertini, F. *Dyes Pigm.* **2013**, *99*, 329.
(62) Huo, E.-F.; Zou, Y.; Sun, H.-Q.; Bai, J.-L.; Huang, Y.; Lu, Z.-Y.; Liu, Y.; Jiang, Q.; Zhao, S.-L. *Polym. Bull.* **2011**, *67*, 843.
(63) Dinçalp, H.; Cimen, O.; Ameri, T.; Brabec, C. J.; Içli, S. *Spectrochim. Acta Mol. Biomol. Spectros.* **2014**, *128*, 197.
(64) Tilley, A. J.; Pensack, R. D.; Lee, T. S.; Djukic, B.; Scholes, G. D.; Seferos, D. S. *J. Phys. Chem. C* **2014**, *118*, 9996.
(65) Handa, N. V.; Mendoza, K. D.; Shirtcliff, L. D. *Org. Lett.* **2011**, *13*, 4724.
(66) Kline, R. J.; McGehee, M. D.; Kadnikova, E. N.; Liu, J.; Fréchet, J. M. J. *Adv. Mater.* **2003**, *15*, 1519.
(67) Kline, R. J.; McGehee, M. D.; Kadnikova, E. N.; Liu, J.; Fréchet, J. M. J.; Toney, M. F. *Macromolecules* **2005**, *38*, 3312.
(68) Zen, A.; Pflaum, J.; Hirschmann, S.; Zhuang, W.; Jaiser, F.; Asawapirom, U.; Rabe, J. P.; Scherf, U.; Neher, D. *Adv. Funct. Mater.* **2004**, *14*, 757.
(69) Johansson, L. B.-Å.; Langhals, H. *Spectrochim. Acta Mol. Biomol. Spectros.* **1991**, *47*, 857.
(70) El-daly, S. A.; Fayed, T. A. *J. Photochem. Photobiol. A: Chem.* **2000**, *137*, 15.
(71) Langhals, H.; Karolin, J.; Johansson, L. B. A. *J. Chem. Soc., Faraday Trans.* **1998**, *94*, 2919.
(72) Würthner, F. *Chem. Commun.* **2004**, 1564.
(73) Fu, J.; Padilha, L. A.; Hagan, D. J.; Van Stryland, E. W.; Przhonska, O. V.; Bondar, M. V.; Slominsky, Y. L.; Kachkovski, A. D. *J. Opt. Soc. Am. B* **2007**, *24*, 67.
(74) Padilha, L. A.; Webster, S.; Przhonska, O. V.; Hu, H.; Peceli, D.; Rosch, J. L.; Bondar, M. V.; Gerasov, A. O.; Kovtun, Y. P.; Shandura, M. P.; Kachkovski, A. D.; Hagan, D. J.; Van Stryland, E. W. *J. Mater. Chem.* **2009**, *19*, 7503.
(75) Kasatani, K.; Kawasaki, M.; Sato, H. *Chem. Phys.* **1984**, *83*, 461.
(76) Niklas, J.; Mardis, K. L.; Banks, B. P.; Grooms, G. M.; Sperlich, A.; Dyakonov, V.; Beaupré, S.; Leclerc, M.; Xu, T.; Yu, L.; Poluektov, O. G. *Phys. Chem. Chem. Phys.* **2013**, *15*, 9562.

DOI: 10.1021/ja513002h
J. Am. Chem. Soc. 2015, 137, 5759−5769